Soft Matter

PAPER

View Article Online
View Journal | View Issue

Cite this: *Soft Matter*, 2015, 11, 6327

Dynamics of fatty acid vesicles in response to pH stimuli†

Keita Ikari,[a] Yuka Sakuma,[a] Takehiro Jimbo,[a] Atsuji Kodama,[a] Masayuki Imai,*[a] Pierre-Alain Monnard[b] and Steen Rasmussen[b]

Received 22nd May 2015,
Accepted 6th July 2015

DOI: 10.1039/c5sm01248a

www.rsc.org/softmatter

We investigate the dynamics of decanoic acid/decanoate (DA) vesicles in response to pH stimuli. Two types of dynamic processes induced by the micro-injection of NaOH solutions are sequentially observed: deformations and topological transitions. In the deformation stage, DA vesicles show a series of shape deformations, *i.e.*, prolate–oblate–stomatocyte-sphere. In the topological transition stage, spherical DA vesicles follow either of the two pathways, pore formation and vesicle fusion. The pH stimuli modify a critical aggregation concentration of DA molecules, which causes the solubilization of DA molecules in the outer leaflet of the vesicle bilayers. This solubilization decreases the outer surface area of the vesicle, thereby increasing surface tension. A kinetic model based on area difference elasticity theory can accurately describe the dynamics of DA vesicles triggered by pH stimuli.

1 Introduction

Amphiphilic vesicles are structures composed of a closed bilayer membrane of amphiphilic molecules. They exhibit unique dynamics in response to external stimuli, such as shear flow, electric field, and optical illumination. Depending on the stimuli type, different dynamic responses are observed, which aim at reducing the stress experienced by the structures. Shear flow causes two characteristic motions of vesicles.[1,2] When an elongational flow is dominant, vesicles exhibit tank-treading motion, whereas tumbling of vesicles is observed, when a rotational flow governs the shear flow. In the presence of electric fields, vesicles are deformed and form transient pores due to the electric stress.[3] An optical illumination of a tubular membrane transforms them into a necklace of pearls to accommodate the increase of surface tension during irradiation.[4]

In contrast to these physical stimuli, chemical stimuli lead to other types of response dynamics since chemicals interact with membrane molecules and modify their chemical nature. For example, when HCl solutions are micro-injected into an anionic phospholipid vesicle, the vesicle membrane forms invaginated tubes.[5–7] The observed membrane deformation is well described by the changes in the equilibrium lipid density and the spontaneous membrane curvature induced by the chemical modification of lipids in the outer leaflet. The micro-injection of NaOH solution into neutral phospholipid vesicles can also induce their movement toward the source of the chemical stimulus.[8] This behaviour might be due to the alkaline hydrolysis of the phospholipids, which decreases the local surface tension of the membrane, driving them toward the region where the surface tension is lower.[9] Thus chemical stimuli have high potential to control vesicle dynamics. So far the dynamics in response to the external stimuli has been investigated using phospholipid vesicles.

The fatty acids, which are composed of a carboxylic acid functional group bonded to a long aliphatic chain, are simple amphiphilic molecules that form vesicles.[10,11] Due to the weak electrolyte nature of these amphiphiles, their vesicles are more sensitive to chemical modifications than their phospholipid counterparts.[12] One important property of the fatty acid assemblies is that their critical aggregation concentration (cac.) is strongly dependent on the pH. For example, the cac of decanoic acid/decanoate (DA) molecules varies from 14 mM at pH 6.8 to 102 mM at pH 11.8.[13] DA molecules are therefore easily solubilized into the medium by increasing the pH. The second important property is that the type of self-assembled structure depends on the pH. In the high pH region, the fatty acids preferentially form micelles, whereas in the low pH region they form oil droplets. The formation of fatty acid vesicles is restricted to a rather narrow pH range (*ca.* 6.8–8 for DA), where approximately half of the carboxylic groups are ionized.[14] These two features induce unique dynamics in the fatty acid vesicles subjected to pH stimuli. The purpose of this study is to investigate the dynamics of fatty acid vesicles in response to pH stimuli and understand their physical basis.

[a] *Department of Physics, Tohoku University, Aramaki, Aoba, Sendai 980-8578, Japan. E-mail: imai@bio.phys.tohoku.ac.jp; Tel: +81 22 795 6464*
[b] *Center for Fundamental Living Technology (FLinT), University of Southern Denmark, 5230 Odense M, Denmark*

† Electronic supplementary information (ESI) available: Videos of dynamics of a fatty acid vesicle in response to pH stimuli. See DOI: 10.1039/c5sm01248a

2 Materials and methods

2.1 Chemicals

Decanoic acid, sodium hydroxide (NaOH) and hydrogen chloride (HCl) in special grade were obtained from Wako pure chemical industries, Ltd (Osaka, Japan). In the experiments, we used purified water obtained from the Direct-Q 3 UV system (Millipore, USA).

2.2 Preparation of DA vesicles

Since the formation of fatty acid vesicles is restricted to the pH range of 6.8–8, usually DA vesicles are prepared by adjusting the pH using buffer solutions.[13] The buffer solutions, however, reduce influences of pH stimuli significantly. We therefore have to prepare DA vesicles without buffer solutions, applying the pH titration method.[15] First, we pipetted 38.7 μl decanoic acid liquid (60 °C) into 4.1 ml pure water (60 °C), which resulted in the formation of DA droplets floating on the water surface. 500 μl NaOH solution (1 M) was then mixed with the DA solution at 60 °C, which solubilized DA droplets (pH 13.0). Thereafter, the transparent DA solution (60 °C) was titrated with 400 μl HCl solution (1 M) using a pipette. The resulting samples were turbid due to the formation of giant vesicles having the sizes of ~10 μm (pH 6.8). The pH stimuli experiments were performed using the vesicle suspension immediately after the sample preparation.

2.3 pH stimuli experiments

A sample chamber for the micro-injection experiments was a hole in a silicon rubber sheet, which was placed onto a glass slide (Fig. 1). The hole had a diameter of 9 mm and a thickness of 1 mm. The micro-pipette used for the micro-injection was a Femtotip II with an inner diameter of 0.5 μm ± 0.2 μm (Eppendorf, Germany). The positioning of the micro-pipette was controlled using a hydraulic micro-manipulator MMO-202ND (Narishige, Japan), and the micro-injection was performed using a FemtoJet system (Eppendorf, Germany). An 65 μl aliquot of the vesicle suspension was carefully transferred into the sample chamber at room temperature. The micro-pipette filled with the injection solution was then inserted into the chamber. To minimize the drift flow in the sample solution, we carefully performed all procedures and waited 10 min for the sample to equilibrate. Most of the injection experiments were performed using an injection pressure of 15 h Pa, and behavior of GVs triggered by the injection was observed using an Axio Observer Z1 inverted fluorescent microscope (Carl Zeiss, Germany) with a 20× objective (Plan-Neofluar 20× N.A. = 0.50) and recorded using a CMOS camera, ORCA-Flash 4.0, with a time resolution of 50 msec (Hamamatsu Photonics, Japan).

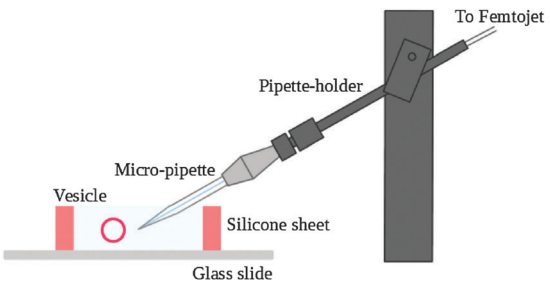

Fig. 1 Experimental setup for a micro-injection experiment.

3 Results and discussion

3.1 pH field generated by micro-injection

In this study, we examined DA vesicle dynamics triggered by the micro-injection of NaOH solutions. The micro-injection produces a pH gradient around the tip of the micro-pipette. The concentration of injected solute $C(x,y,z,t)$ at position (x,y,z) and time t was calculated by solving the diffusion equation with convoluting the inner radius of the pipette, ε, as

$$C(x,y,z,t) = \int_0^t\int_0^{\varepsilon}\int_0^{2\pi} \frac{S_0 \exp\left[-\dfrac{(x-r\cos\theta)^2+(y-r\sin\theta)^2+(z-z_0)^2}{4D(t-s)}\right]}{4\pi D(t-s)^{3/2}} r\,\mathrm{d}r\,\mathrm{d}\theta\,\mathrm{d}s \quad (1)$$

where S_0 is the flux of the injected OH^- from the pipette, D is the diffusion coefficient of the solute, r and θ designate the position in the mouth of the pipette and the pipette axis is the z direction.[8] The position of the micro-pipette tip is (0,0,0). The time dependence of the pH profiles was calculated for a micro-injection of 50 mM NaOH solution, using $D_{OH} = 5.27 \times 10^{-9}$ m^2 s^{-1} and $S_0 = 2.15 \times 10^{-18}$ mol s^{-1} (Fig. 2).[16] The concentration of OH^- steeply decreases in the vicinity of the tip and thereafter gradually decreases with an increasing distance from the tip. Overtime, the OH^- concentration increases at distances larger than ~5 μm and the profiles reach a steady state within ~1 s. At the distances larger than ~15 μm, the pH gradient in the steady state is not significant, *i.e.*, vesicles feel a constant pH. It should be noted that the micro-injection generates injection flow around the micro-pipette. We visualized the injection flow using small aggregates of DA dispersed in the medium. The obtained velocities of the injection flow were ~1 μm s^{-1} in

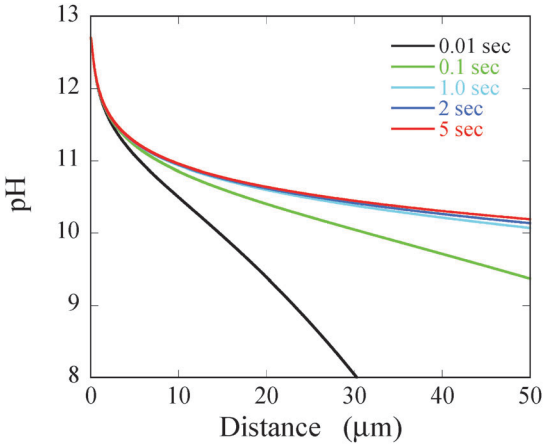

Fig. 2 Time dependence of the pH profile around the tip of the micro-pipette (located at a distance of 0 μm) after the continuous micro-injection of a 50 mM NaOH solution calculated by eqn (1).

the vicinity of the tip and negligible at the distances larger than ~10 μm. This velocity is much smaller than the diffusion length per s of hydroxide ions, $\sim\sqrt{D_{OH}t} = 73$ μm. Effects of the injection flow can be therefore neglected.

We chose to focus on the micro-injection of 50 mM NaOH solution (pH 12.7) as the vesicle dynamics observed at this pH were representative for the injection of any NaOH solution pH ≥11, while the effects of solution with pH 5 to 11 on the vesicle morphology were limited. Only vesicles located at distances larger than ~15 μm from the tip were studied, because these vesicles are exposed to a constant pH value of ~10.7. Two types of dynamic processes were observed: deformations and topological transitions.

3.2 Deformations

An important effect of the micro-injection of basic solution is the solubilization of DA molecules in the outer leaflet, since the cac of DA molecules increases with increase of the pH and the pH stimuli are applied only on the outer leaflet. This asymmetric solubilization causes unique shape deformations of the vesicles. A representative shape deformation pathway of vesicles subjected to the micro-injection of 50 mM NaOH is shown in Fig. 3(a) and video S1 of the ESI.† The distance between the vesicle and the tip of the micro-pipette was ~20 μm. By the micro-injection, a prolate vesicle kept its shape for ~1 s and then transformed into a stomatocyte shape *via* an oblate shape. Subsequently, the stomatocyte vesicle deformed to a sphere with regressing invagination. The spherical vesicle decreased its size overtime and finally disappeared due to the micellisation, as expected for deprotonated fatty acids. We repeated the micro-injection experiments more than 10 times, always observing dynamics comparable to those presented here.

First, we discuss the observed shape deformation from prolate to sphere based on the area difference elasticity (ADE) theory,[17–19] since ADE theory accurately describes vesicle shapes and shape transitions.[20] The elastic energy of ADE theory normalized by the bending energy of a sphere is expressed by

$$\begin{aligned}\frac{W}{8\pi\kappa_c} &= \frac{1}{8\pi\kappa_c}\left[\frac{\kappa_c}{2}\int(2H)^2 dA + \frac{\kappa_r}{2Ad^2}(\Delta A - \Delta A_0)^2\right] \\ &= \frac{1}{16\pi}\int(2H)^2 dA + \frac{\kappa_r}{\kappa_c}(\Delta a - \Delta a_0)^2,\end{aligned} \quad (2)$$

where κ_c and κ_r are the local and the non-local bending moduli, respectively, H is the mean curvature, and A is the vesicle area. The geometrical area difference between the inner and the outer leaflet, ΔA, is given by

$$\Delta A = 2d\oint H dA, \quad (3)$$

where d is the distance between the neutral surfaces of monolayers and the intrinsic area difference, ΔA_0, is given by

$$\Delta A_0 = (N^+ - N^-)a, \quad (4)$$

where N^+ and N^- are the number of DA molecules in the outer and the inner leaflet, respectively. a = 0.226 nm^2 is the cross section area of a DA molecule (for simplicity we assume that a decanoic acid molecule and a decanoate molecule have the same cross section area).[21,22] The ADE energy arises from the deviation in the total area difference ΔA from ΔA_0. The two area differences, ΔA and ΔA_0, are normalized by the area difference of a sphere as

$$\Delta a = \frac{\Delta A}{8\pi d R_0} \quad (5)$$

$$\Delta a_0 = \frac{\Delta A_0}{8\pi d R_0}, \quad (6)$$

where $R_0 = \sqrt{A/4\pi}$. The vesicle shape is obtained by minimization of the elastic energy, eqn (2), with constant volume, V,

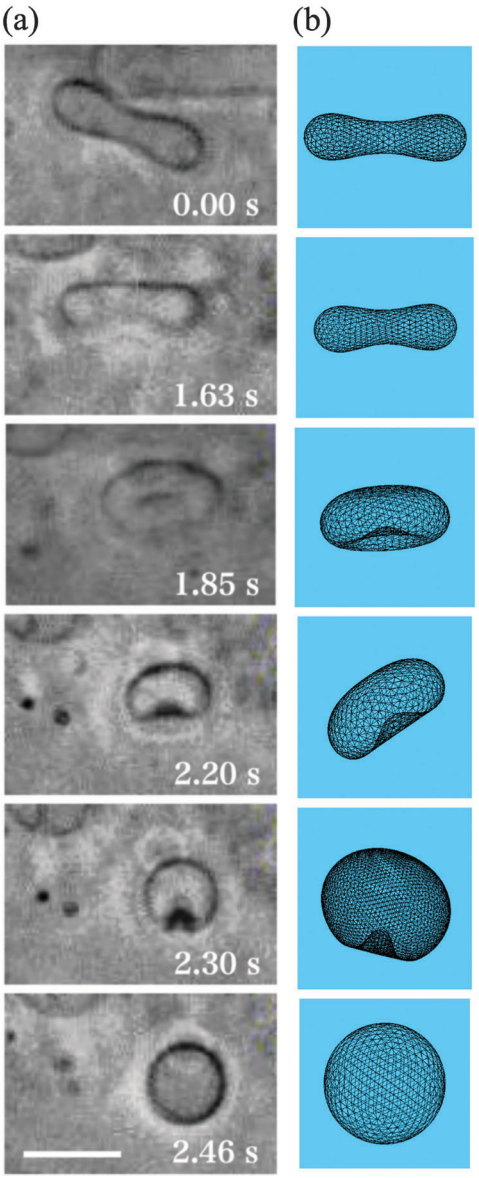

Fig. 3 (a) A series of shape deformations of DA vesicles triggered by micro-injection of 50 mM NaOH. Elapsed time since the injection start (0.00 s) is shown at the bottom corner of each image. A scale bar is 5 μm. See also video S1 in the ESI,† which shows real time deformation (injection was started at 7.00 s in the video S1, ESI†). (b) Reconstructed 3D vesicle image for each microscope image obtained by a surface evolver package.

and constant area, A, constraints. According to ADE model vesicle shapes are determined by two geometrical parameters, the reduced volume given by $v = V/[4\pi R_0^3/3]$ and the normalized intrinsic area difference, Δa_0. A morphology diagram obtained by the ADE model (κ_r/κ_c = 4.4) is shown in Fig. 4. The ratio κ_r/κ_c = 4.4 is usually used to describe phospholipid vesicle morphologies[18,20] and we assume that this ratio is also valid for fatty acid vesicles. Solid lines indicate the first-order discontinuous transitions between stomatocyte and oblate ($D^{sto/obl}$), oblate and prolate ($D^{obl/pro}$), and prolate and pear ($D^{pro/pea}$). A limiting shape line is shown by L. The shape transition (*e.g.* from prolate to oblate) should take place when the deformation trajectory crosses the shape boundary line ($D^{obl/pro}$).

We estimate the shape deformation trajectory based on the asymmetric solubilization model illustrated in Fig. 5. DA molecules in an outer leaflet are solubilized into the external medium with a rate constant of k_s, whereas DA molecules in an inner leaflet undergo a flip-flop motion with a rate constant of k_f. This kinetic model is described by the following differential equations,

$$\frac{dN^+}{dt} = -k_s N^+ + k_f N^- \quad (7)$$

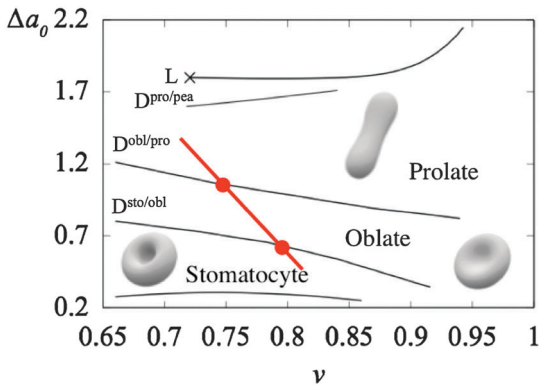

Fig. 4 Morphology diagram in the (v, Δa_0) plane predicted by the ADE model with κ_r/κ_c = 4.4. Solid lines indicate first-order discontinuous transitions between stomatocyte and oblate ($D^{sto/obl}$), oblate and prolate ($D^{obl/pro}$), and prolate and pear ($D^{pro/pea}$). A limiting shape line is shown by L. The schematic vesicle image of each phase is shown. Thick red line is a predicted trajectory for vesicle 1 (deformation process shown in Fig. 3) based on a kinetic model described in text and the transition points are marked by red circles.

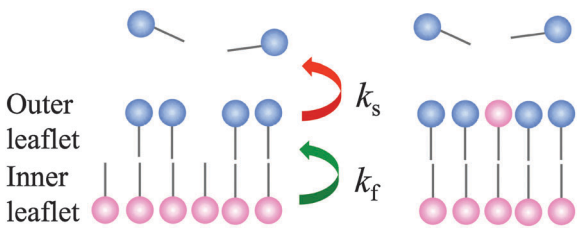

Fig. 5 A schematic representation of a kinetic model for the deformation stage. DA molecules in an outer leaflet are solubilized into the external medium with a rate constant of k_s, whereas DA molecules in an inner leaflet undergo a flip-flop motion with a rate constant of k_f.

$$\frac{dN^-}{dt} = -k_f N^- . \quad (8)$$

The simultaneous differential equations can be solved as

$$N^+(t) = N^+(0)\exp(-k_s t) + N^-(0)(1 - \exp(-k_f t)) \quad (9)$$

$$N^+(t) = N^+(0)\exp(-k_f t). \quad (10)$$

Then time dependence of the total surface area of a vesicle is expressed by

$$\begin{aligned} A(t) \cong A_0(t) &= \frac{N^+(t) + N^-(t)}{2}a \\ &= \frac{N^+(0)\exp(-k_s t) + N^-(0)}{2}a \\ &\simeq A_0(0)\left(1 - \frac{k_s}{2}t\right), \end{aligned} \quad (11)$$

since the area difference is much smaller than the total area of the vesicle. Thus the vesicle area linearly decreases with time and the slope gives the solubilization rate. However, the volume of a vesicle keeps a constant value during the deformation stage.

To validate this prediction, we evaluate time dependencies of the total area and volume of vesicles. We reconstructed stable 3D vesicle shapes from the observed 2D images by using a surface evolver (SE) package,[23] where we assume that vesicles have axisymmetric shapes. The stable vesicle shapes were obtained by minimizing the ADE energy, eqn (2). The accuracy of the 3D vesicle model was first assessed by visual inspection and then by using a calculated parameter, the ratio of the vesicle height to width.[24] Reconstructed stable 3D vesicle images are displayed in Fig. 3(b). Within the SE package, we can readily evaluate vesicle volume V and area A, as well as the geometrical area difference ΔA.

Fig. 6(a) shows obtained time dependencies of A and V for the deformation of three vesicles, where the origin of time is the start time of the micro-injection. Please note that the deformation process for vesicle 1 is illustrated in Fig. 3. For all deformation pathways, the vesicle area was kept constant during the first 1 s and then decreased linearly with time. The time lag, t_0, originates from the time interval between the injection and the induction of the vesicle changes due to diffusion as highlighted in Fig. 2. After this lag phase, vesicles felt the steady pH field around the pipette (pH $\sim$ 10.7). While the vesicle volume was kept constant, $V(t_0)$, the observed decrease of the vesicle areas (Fig. 6(a)) for three deformation examples was fitted by eqn (11) with an offset time of t_0 = 1.0 s, which gives the solubilization rate, $k_s = 0.28 \pm 0.03\ s^{-1}$.

We also plot the reduced volume of vesicle 1, obtained from the total area and the volume of the vesicle calculated by SE, as a function of time in Fig. 6(b). Using eqn (11) the time dependence of the reduced volume is expressed by

$$v(t - t_0) = \frac{3V(t_0)}{4\pi\left[\frac{A(t_0)}{4\pi}\left(1 - \frac{k_s(t - t_0)}{2}\right)\right]^{\frac{3}{2}}}, \quad (12)$$

which is shown by a solid line in Fig. 6(b). Here, $A(t_0)$ and $V(t_0)$ are the area and the volume of vesicle 1 at $t = t_0$ (=1 s).

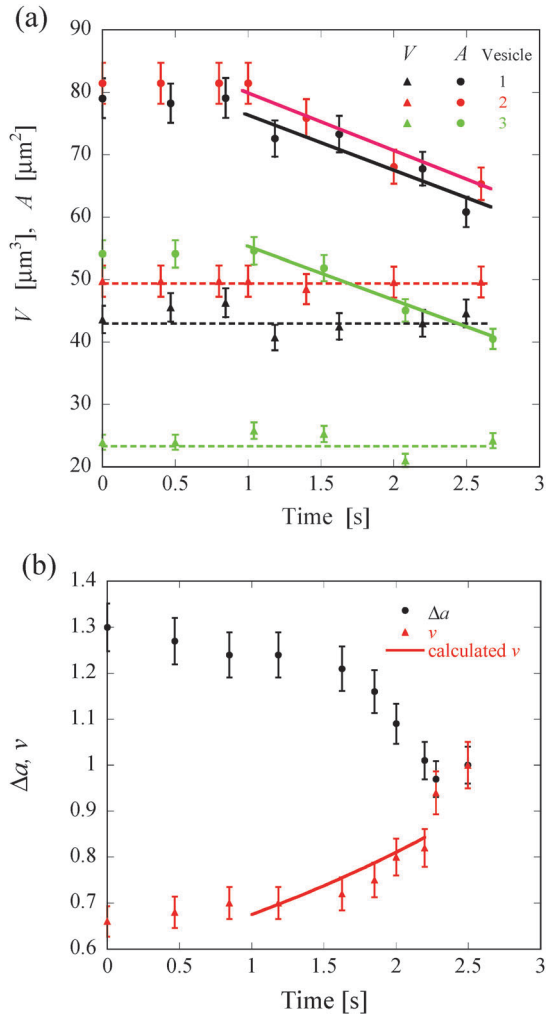

Fig. 6 (a) Time dependences of total area (closed circles) and volume (closed triangles) of three vesicles (1–3) in the deformation stage (the deformation process of vesicle 1 is shown in Fig. 3). Solid lines are results of fitting for time dependencies of total area using eqn (11) and broken lines indicate that volume of each vesicle keeps a constant value during the deformation stage. (b) Time dependence of the geometrical area difference (black closed circles) and the reduced volume (red closed triangles) in the deformation stage of vesicle 1. A solid line is the predicted time dependence of the reduced volume using eqn (12) with t_0 = 1 s.

The calculated reduced volume agrees with the experimental data. In addition, we obtained the normalized geometrical area differences, Δa, from the stable 3D vesicle images of vesicle 1 and plot them as a function of time in Fig. 6(b). The initial shape (t = 1 s) of the vesicle 1 was a prolate having values of (Δa, v) ~ (1.25, 0.7). The vesicle 1 kept the prolate shape until t ~ 1.6 s and it then transformed into oblate shape with (Δa, v) ~ (1.16, 0.75) at t ~ 1.85 s. Subsequently, the oblate vesicle adopted a stomatocyte shape with (Δa, v) ~ (1.09, 0.80) at t ~ 2.0 s. Finally, this stomatocyte vesicle converted into a spherical shape with (Δa, v) ~ (1.0, 1.0). As described above, shape transitions from prolate to oblate and from oblate to stomatocyte should take place when the deformation trajectory in the (Δa_0, v) plane crosses the discontinuous transition lines between prolate and oblate ($D^{pro/obl}$), and between oblate and stomatocyte ($D^{obl/sto}$), respectively (Fig. 4). Using the reduced volumes at the prolate/oblate transition (v = 0.75) and the oblate/stomatocyte transition (v = 0.8), we can fix the transition points on the discontinuous transition lines in the (v, Δa_0) phase diagram (Fig. 4), thereby the trajectory of vesicle 1 across the $D^{pro/obl}$ line at (v, Δa_0) = (0.75, 1.0), and the $D^{obl/sto}$ line at (0.80, 0.6).

Based on the kinetic model the time dependence of the normalized intrinsic area difference is expressed by

$$\Delta a_0(t - t_0) \cong \frac{A_0(t - t_0) - A_0^-(t_0)\exp(-k_f(t - t_0))}{4\pi d\sqrt{A_0(t - t_0)/4\pi}}, \quad (13)$$

where $A_0^-(t_0) = N^-(t_0)a$ is the intrinsic area of the inner leaflet at $t = t_0$. By solving simultaneous equations of eqn (13) at the two transition points (t, Δa_0) = (1.8, 1.0) and (2.0, 0.6), k_f = 0.09 s^{-1} and $A_0^-(t_0)$ = 76.2 μm^2 were obtained, assuming d = 1.71 nm[25,26] and $A_0(t - t_0)$ = 76.3(1 − 0.115($t - t_0$)) μm^2. Using eqn (12) and (13), the deformation trajectory of vesicle 1 in the phase diagram therefore can be determined (Fig. 4). Similarly, k_f = 0.088 s^{-1} and 0.10 s^{-1} were calculated for vesicles 2 and 3 in Fig. 6(a), respectively. Thus, the flip-flop rate of DA molecules is k_f = 0.09–0.10 s^{-1}. This value is smaller than the reported flip-flop rate of 1–10 s^{-1} for fatty acid,[27] but it could be related to the fact that we only observe a net flow of DA molecules from the inner leaflet to the outer leaflet to compensate the loss of DA molecules in the outer leaflet due to the solubilization. Our kinetic model explains the observed vesicle deformation and gives two important time constants for the solubilization and the flip-flop motion.

3.3 Topological transitions

During the solubilization, the total membrane area decreases while the volume is kept constant (Fig. 6(a)), *i.e.*, increase of the reduced volume, and finally vesicles transform into a tense spherical shape. After the deformation to a spherical vesicle, DA molecules continue to dissolve in water, which results in an increase of the membrane tension. To release the membrane tension, the tense vesicles employed two processes: pore formation and fusion. The membrane tension induced pore formation has been reported in many phospholipid vesicle systems including solubilization by detergents.[28–33] In this case, the surface tension of the vesicle increases until it reaches a tension threshold value, *i.e.*, the rupture tension, where a pore with a diameter of up to several μm forms allowing the inner solution to flow out. Thereafter, the radius of the vesicle decreases with time continuously or periodically.[30–32] In the case of DA vesicles, the continuous shrinking of spherical vesicles was observed upon micro-injection of a 50 mM NaOH solution. Fig. 7 shows the shrinking of the tense spherical vesicle (video S2 of the ESI†). In more than ten observations, the vesicle size continuously decreased before the structure finally disappears. Pores on the vesicle could not be directly observed, indicating that the pore radius might be of the order of ~0.1 μm, *i.e.*, below the microscope resolution. However, the formation of a pore is supported by the observation made on shrinking vesicles that encapsulate another vesicle.[31,32]

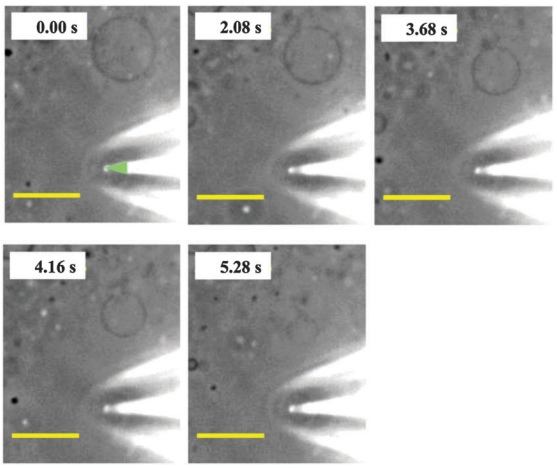

Fig. 7 Shrinking of a spherical DA vesicle triggered by micro-injection of 50 mM NaOH. Elapsed time since spherical vesicle started to shrink is shown at the top corner of each image. A scale bar is 10 μm. See also video S2 in the ESI,† which shows real time shrinking (shrinking was started at 7.84 s in the video).

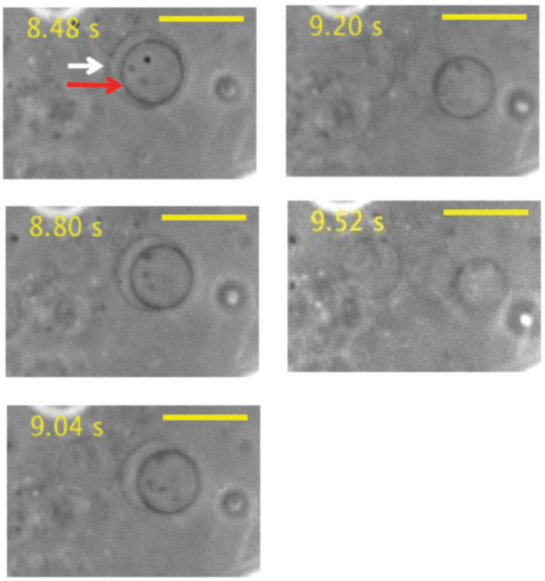

Fig. 8 Exit of a large encapsulated vesicle through a pore. Elapsed time since start of micro-injection (0.0 s) is shown at the top corner of each image. The large vesicle with the radius of ~3.5 μm (red long arrow) was initially inside the mother vesicle with radius of ~4.5 μm (white arrow) (8.48 s). Following the micro-injection, the encapsulated vesicle plugged the pore (8.80 s) and then expanded the pore (9.04 s). Finally, the inside vesicle passed through the pore and a mother vesicle with a radius of ~3 μm and a daughter vesicle with a radius of ~3.5 μm (9.20 s) could be observed. Once separated, both vesicles started to shrink (9.52 s). A scale bar is 10 μm. See also video 3 in the ESI,† which shows the real time exit of encapsulated vesicles.

Fig. 8 illustrates the prototypical response of such a vesicle subjected to the micro-injection of NaOH solution (video S3 of the ESI†). Upon NaOH injection into a spherical vesicle (white arrow) containing another encapsulated vesicle (red long arrow), the inside vesicle was dragged toward the membrane, indicating leaking of the internal fluid through a pore. The inside vesicle plugged the pore and then expanded it. Finally, the encapsulated vesicle passed through the pore and two independent vesicles co-existed. This phenomenon strongly supports the pore formation induced by the solubilization of DA molecules.

When the shrinking of vesicle is governed by the pore formation, the volume of the vesicle varies as

$$\frac{dV}{dt} = -\pi r^2 v_l = 4\pi R^2 \frac{dR}{dt}, \quad (14)$$

where r is the radius of a circular pore on the spherical vesicle with the radius R, and v_l is the leaking velocity of inner solution through the pore. The leaking velocity is determined by the pressure difference between the inner and outer media, ΔP, and the drag force, as

$$v_l = \frac{r(t)\Delta P(t)}{3\pi\eta_s} = \frac{2\sigma(t)r(t)}{3\pi R(t)\eta_s}, \quad (15)$$

where η_s is the viscosity of the solution, and $\sigma(t)$ is the surface tension.[29,34] Combining eqn (14) and (15), we obtain

$$\frac{dR}{dt} = -\frac{\sigma(t)}{6\pi\eta_s}\left(\frac{r(t)}{R(t)}\right)^3. \quad (16)$$

Thus, relative pore size, $r(t)/R(t)$, is determined by the vesicle shrinking rate, dR/dt, and the surface tension.

Fig. 9 shows the time dependence of the vesicle radius at the shrinkage stage, where the start time of the shrinking of spherical vesicle is $t = 0$. As described in the Deformation section, the time dependence of total vesicle area should be expressed by eqn (11). The inset of Fig. 9 shows the time dependence of the surface area, which is well described by the linear function (solid line)

$$A(t) = 290 \times 10^{-12}(1 - 0.132t)\ [\mathrm{m}^2]. \quad (17)$$

Using eqn (11) the slope gives the solubilization rate, k_s = 0.264 s^{-1}. The good agreement in k_s between the deformation stage and the shrinking stage indicates that the solubilization rate does not significantly depend on the membrane tension. From eqn (17) the shrink rate can be expressed by dR/dt = $1.25 \times 10^{-12}/R$ m s^{-1} and the pore/vesicle size ratio, $r(t)/R(t)$, is then given by

$$\left(\frac{r(t)}{R(t)}\right)^3 = \frac{1.52 \times 10^{-12}}{R}\frac{6\pi\eta_s}{\sigma(t)}. \quad (18)$$

Since we cannot observe a definite pore on the vesicle, this ratio should be less than 0.1, $r(t)/R(t) \leq 0.1$. The surface tension has then to be larger than 10^{-5} N m^{-1}, which is larger than that of the phospholipid vesicle with a long-lasting pore ($\sigma \sim 10^{-6}$ N).[32] The high solubilization rate of DA molecules (k_s = 0.26 s^{-1}) for the pH stimulus might explain the high surface tension.

Another important dynamics to release the tension is fusion between two tense vesicles. An example of the fusion event is shown in Fig. 10 and video S4 of the ESI.† When two tense, adjacent vesicles were subjected to the micro-injection of 50 mM NaOH, these vesicles could suddenly fuse and form one larger spherical vesicle over a transient budding shape.

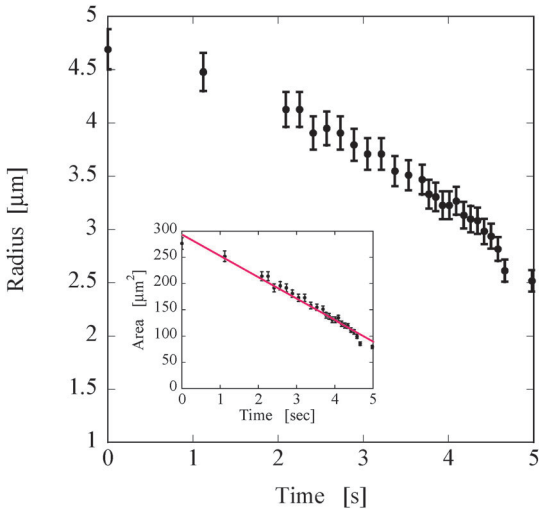

Fig. 9 Time dependence of the vesicle radius in the shrinking stage of the vesicle shown in Fig. 7. The origin of time is when the spherical vesicle started to shrink. The inset is time dependence of the vesicle area. A solid line is a result of fitting using eqn (11).

During this fusion, the total area of the vesicle decreased from $\sim$360 μm^2 (two vesicles) to $\sim$290 μm^2 (a single vesicle), whereas the volume kept a constant value of $\sim$460 μm^3, *i.e.*, without leaking of the inner solution. The excess membrane produced by the fusion clung to the fused spherical vesicle as a black patch at the contact zone (arrow in Fig. 10, 5.12 s). Dissipative particle dynamics simulations propose the following dynamics of tension-induced vesicle fusion.[35–37] The energy barrier that prevents the fusion of vesicles is related to the energy cost of inter-membrane amphiphilic molecule flips between the adjacent vesicles. This energy barrier should be reduced by increasing the surface tension since the amphiphilic molecule distance in a layer increases with the tension. The inter-membrane flips are consequently accelerated. The intermingling of the amphiphilic molecules in apposing bilayers generates a hemifused-bilayer zone. This zone grows due to the surface tension and finally forms the fusion pore, resulting in the vesicle fusion. Unfortunately, due to limits of the length and time resolution, we could not visualize the fusion mechanism. However, our observations clearly show the tension induced vesicle fusion, because fusion events between adjacent spherical vesicles never occurred in the time frame of the observation without the micro-injection of NaOH solution. After the fusion the spherical vesicles exhibited morphological changes consistent with those of the shrink pathway by pore formation.

We have shown that the pH stimulus induces two types of dynamics in DA vesicles; deformations and topological transitions. The main effect of the pH stimuli on DA vesicles is the solubilization of DA molecules in the outer leaflet of the vesicle bilayers. This solubilization is responsible for the observed deformations and topological transitions. The observed dynamics is characteristic of fatty acid vesicles, since the critical aggregation concentration of fatty acids increases with increase of pH. For phospholipid vesicles we did not observe the similar dynamics caused by the solubilization of phospholipids. The main effects of

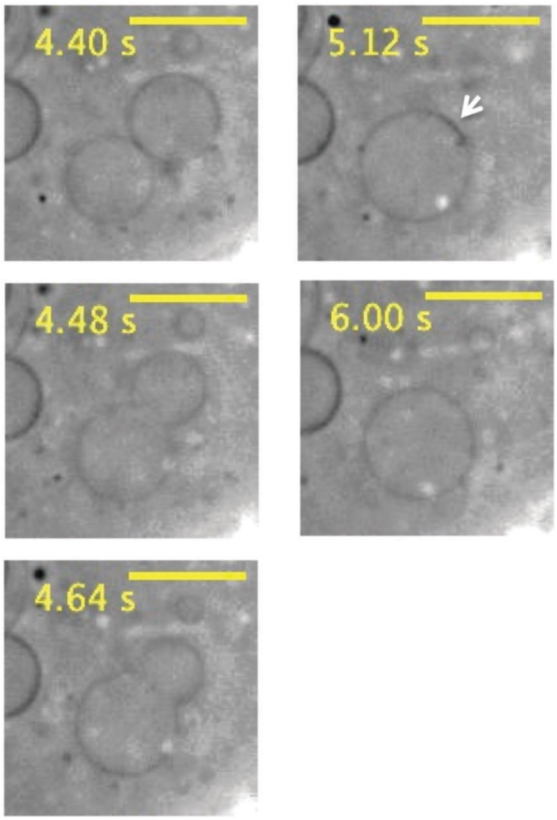

Fig. 10 Fusion of two spherical DA vesicles triggered by the micro-injection of 50 mM NaOH. Elapsed time since start of the micro-injection (0.0 s) is shown at the top corner of each image. An arrow in the 5.12 s frame shows the clung membrane at the contact zone. A scale bar is 10 μm. See also video S4 in the ESI,† which shows the real time fusion process.

the pH stimuli on the phospholipid vesicle are modifications of the shape of lipid molecules and the surface tension. The former effect induces the formation of the tubular membrane,[5–7] whereas the latter effect causes the migration of the vesicle to decrease the surface energy.[8] Thus effects of the pH stimuli on vesicles depend on the types of amphiphilic molecules that compose the vesicle.

4 Conclusions

By applying pH stimuli to DA vesicles, two types of unique response dynamics caused by the solubilization of DA molecules are observed: deformations and topological transitions. In the deformation stage, a coupling of solubilization of DA molecules in the outer leaflet and the flip-flop motion from the inner to the outer leaflet causes a series of shape deformations, *i.e.*, prolate–oblate–stomatocyte-sphere. The kinetic model based on the area difference elasticity (ADE) theory quantitatively describes the observed shape deformations and gives two characteristic time constants, the solubilization and the flip-flop rates. In the topological transition stage, the solubilization of DA molecules out of spherical vesicles increases the membrane tension. To release the tension, vesicles can follow two pathways: pore formation and vesicle fusion, two topological transitions that are relevant to transportation

processes in a cellular system. The observed dynamics of fatty acid vesicles in response to the pH stimuli highlight the uniqueness of chemical stimuli to control the vesicle shape. Moreover fatty acids are considered plausible prebiotic amphiphiles.[38] That is, precellular compartments may be modelled by fatty acid vesicles. The vesicle dynamics induced by chemical stimuli may have therefore played a significant role in the evolution of molecular, self-assembled, precellular systems toward the cellular life.[39]

Acknowledgements

It is our pleasure to acknowledge discussions with P. Ziherl (University of Ljubljana, Jožef Stefan Institute) for 3D analysis of vesicles. We thank Toshihiro Kawakatsu (Tohoku university) and Yutaka Oya (Tohoku University) for helpful suggestions. This work was in part supported by Grant-in-Aid for Scientific Research (A) 22244053, 25247070, Grant-in-Aid for Scientific Research on Innovative Areas "Fluctuation and Structure" (No. 25103009), the Core-to-Core Program "Non-equilibrium dynamics of soft matter and information" from the Japan Society for the Promotion of Science as well as the European Commission sponsored projects MICREAgents, TRUCE and Synenergene.

References

1 S. Braunmüller, L. Schmid, E. Sackmann and T. Franke, *Soft Matter*, 2012, **8**, 11240.
2 J. Deschamps, V. Kantsler, E. Segre and V. Steinberg, *Proc. Natl. Acad. Sci. U. S. A.*, 2009, **106**, 11444.
3 K. A. Riske and R. Dimova, *Biophys. J.*, 2005, **88**, 1143.
4 R. Bar-Ziv and E. Moses, *Phys. Rev. Lett.*, 1994, **73**, 1392.
5 N. Khalifat, N. Puff, B. Bonneau, J. B. Fournier and M. I. Angelova, *Biophys. J.*, 2008, **95**, 4924.
6 J. B. Fournier, N. Khalifat, N. Puff and M. I. Angelova, *Phys. Rev. Lett.*, 2009, **102**, 018102.
7 A. F. Bitbol, N. Puff, Y. Sakuma, M. Imai, J. B. Fournier and M. I. Angelova, *Soft Matter*, 2012, **8**, 6073.
8 A. Kodama, Y. Sakuma, M. Imai, T. Kawakatsu, N. Puff and M. I. Angelova, *Phys. Rev. E.*, submitted.
9 J. L. Anderson, *Annu. Rev. Fluid Mech.*, 1989, **21**, 61.
10 J. M. Gebicki and M. Hicks, *Nature*, 1973, **243**, 232.
11 J. M. Gebicki and M. Hicks, *Chem. Phys. Lipids*, 1976, **16**, 142.
12 K. Morigaki and P. Walde, *Curr. Opin. Colloid Interface Sci.*, 2007, **12**, 75.
13 K. Morigaki, P. Walde, M. Misran and B. H. Robinson, *Colloids Surf., A*, 2003, **213**, 37.
14 D. P. Cistola, D. Atkinson, J. A. Hamilton and D. M. Small, *Biochemistry*, 1986, **25**, 2804.
15 P.-A. Monnard and D. W. Deamer, *Methods Enzymol.*, 2003, **372**, 133.
16 E. L. Cussler, *Diffusion – Mass Transfer in Fluid Systems*, Cambridge University Press, 2009.
17 V. Heinrich, S. Svetina and B. Žekš, *Phys. Rev. E: Stat. Phys., Plasmas, Fluids, Relat. Interdiscip. Top.*, 1993, **48**, 3112.
18 M. Jarić, U. Seifert, W. Wintz and M. Wortis, *Phys. Rev. E: Stat. Phys., Plasmas, Fluids, Relat. Interdiscip. Top.*, 1995, **52**, 6623.
19 U. Seifert, *Adv. Phys.*, 1997, **46**, 13.
20 A. Sakashita, N. Urakami, P. Ziherl and M. Imai, *Soft Matter*, 2012, **8**, 8569.
21 R. E. Heikkila, C. N. Kwong and D. G. Cornwell, *J. Lipid Res.*, 1979, **11**, 190.
22 K. D. Danov, P. A. Kralchevsky, K. P. Ananthapadmanabhan and A. Lips, *J. Colloid Interface Sci.*, 2006, **300**, 809.
23 K. Brakke, *Exp. Math.*, 1992, **1**, 141–165, the software package is available free of charge at http://www.susqu.edu/brakke/evolver/evolver.html.
24 J. Majhenc, B. Božič, S. Svetina and B. Žekš, *Biochim. Biophys. Acta*, 2004, **1664**, 257.
25 C. Tanford, *The Hydrophobic Effect: Formation of Micelles and Biological Membranes*, Wiley, New York, 2nd edn, 1980.
26 P. C. Hiemenz and R. Rajagopalan, *Principles of Colloid and Surface Chemistry*, Dekker, New York, 3rd edn, 1997.
27 J. A. Hamilton, *J. Lipid Res.*, 1998, **39**, 467–481.
28 O. Sandre, L. Moreaux and F. Brochard-Wyart, *Proc. Natl. Acad. Sci. U. S. A.*, 1999, **96**, 10591.
29 F. Brochard-Wyart, P. G. de Gennes and O. Sandre, *Physica A*, 2000, **278**, 32.
30 F. Nomura, M. Nagata, T. Inaba, H. Hiramatsu, H. Hotani and K. Takiguchi, *Proc. Natl. Acad. Sci. U. S. A.*, 2001, **98**, 2340.
31 E. Karatekin, O. Sandre, H. Guitouni, N. Borghi, P.-H. Puech and F. Brochard-Wyart, *Biophys. J.*, 2003, **84**, 1734.
32 N. Rodriguez, S. Cribier and F. Pincet, *Phys. Rev. E: Stat., Nonlinear, Soft Matter Phys.*, 2006, **74**, 061902.
33 T. Hamada, Y. Hirabayashi, T. Ohta and M. Takagi, *Phys. Rev. E: Stat., Nonlinear, Soft Matter Phys.*, 2009, **80**, 051921.
34 M. A. Idiart and Y. Levin, *Phys. Rev. E: Stat., Nonlinear, Soft Matter Phys.*, 2004, **69**, 061922.
35 J. C. Shillcock and R. Lipowsky, *Nat. Mater.*, 2005, **4**, 225.
36 A. Grafmüller, J. Shillcock and R. Lipowsky, *Phys. Rev. Lett.*, 2007, **98**, 218101.
37 L. Gao, R. Lipowsky and J. Shillcock, *Soft Matter*, 2008, **4**, 1208.
38 P.-A. Monnard and D. W. Deamer, in *The Minimal Cell*, ed. P. L. Luisi and P. Stano, Springer, Heidelberg, 2011.
39 *Protocells: Bridging Nonliving and Living Matter*, ed. S. Rasmussen, M. A. Bedau, L. Chen, D. Deamer, D. C. Krakauer, N. H. Packard and P. F. Stadler, The MIT Press, Cambridge, 2009.

